Scientia Iranica F (2013) 20(6), 2314–2322

SCIENTIA IRANICA

Sharif University of Technology

Scientia Iranica

Transaction F: Nanotechnology

www.scientiairanica.com

Stability analysis of boron nitride nanotubes via a combined continuum-atomistic model

R. Ansari, H. Rouhi* and M. Mirnezhad

Department of Mechanical Engineering, University of Guilan, Rasht, P.O. Box 41635-3756, Iran.

Received 29 August 2012; received in revised form 8 December 2012; accepted 6 May 2013

KEYWORDS

Boron nitride nanotube;
Elastic buckling;
Continuum mechanics;
Molecular mechanics;
Density functional theory.

Abstract. A hybrid continuum-atomistic approach is developed to describe the buckling behavior of axially loaded chiral boron nitride nanotubes (BNNTs) with different boundary conditions. The set of the stability equations is established based on the nonlocal elasticity of Eringen and Donnell shell theory. The molecular mechanics are implemented in conjunction with the Density Functional Theory (DFT) to obtain the effective in-plane and bending stiffnesses and Poisson's ratio of BNNTs. The problem is analytically solved by the use of a direct variational method. The influences of geometrical parameters, nonlocal parameters and boundary conditions on the critical buckling loads are thoroughly explored.

1. Introduction

BNNTs, as the structural analogues of carbon nanotubes (CNTs) [1], since their discovery in the middle of 1990s [2-4], have attracted increasing interest in nanoscience and nanotechnology. They possess high thermal conductivity [5], size-dependent electronic, magnetic and piezoelectricity properties [6-8], high temperature resistance to oxygen [9] and demonstrate a promise for structural reinforcement of matrix materials [10]. Numerous theoretical studies on the mechanical properties of BNNTs have been conducted by a number of researchers [11-18]. Chopra and Zettl [19], via thermal vibration analysis, indicated that Young's modulus of multi-walled BNNTs is in the order of 1 TPa (1.22 ± 0.24 TPa). Furthermore, contrary to CNTs, BNNTs are all semiconductors with a large band gap (~ 5.5 eV), regardless of chirality and size [3,20]. Also, Golberg et al. [21] showed that BNNTs buckle in equilibrated structures because of the different surface energies of boron and nitrogen atoms.

To study the mechanical behavior of nanostructures theoretically, molecular mechanics and continuum mechanics are two promising approaches. Molecular mechanics models have attracted much research interest in recent years. They have been used to analytically study the mechanical response of nanotubes [18,22-25]. Since classical continuum theory is size-independent, several attempts have been made to develop higher-order continuum theories capable of capturing size effects. One way to incorporate nanoscale size effects into continuum mechanics models is the use of the nonlocal elasticity theory [26,27]. The application of nonlocal continuum mechanics, allowing for small scale effects, has been recommended by many researchers [28-37].

The results of continuum models depend on the applied values of mechanical properties, such as Young's modulus and Poisson's ratio. In a recent work by Ansari and Rouhi [37] on the vibrations of CNTs, based on a nonlocal Flugge shell model, it is revealed that the variation of Young's modulus significantly affects the value of the nonlocal parameter, so as to get a close fit with molecular dynamics results. Motivated by this consideration, in the current work, a hybrid of continuum and molecular mechanics is applied to

*. *Corresponding author. Tel./Fax: +98 131 6690276*
E-mail address: rouhi.hessam@gmail.com (H. Rouhi)

investigate the axial buckling behavior of single-walled BNNTs under different end conditions. To this end, first, a nonlocal shell model is developed on the basis of Eringen's elasticity and the Donnell shell theory. In the context of calculus of variation, the Rayleigh-Ritz procedure is implemented in the variational statement derived from the Donnell-type buckling equations to analytically solve the problem. Subsequently, in order to determine the precise values of effective in-plane and bending stiffnesses and Poisson's ratio of BNNTs with various chiralities, molecular mechanics theory is used in conjunction with DFT calculations.

2. Nonlocal shell model

Consider an elastic cylindrical shell with radius, R, and thickness, h, as illustrated in Figure 1. In contrast to classical elasticity, in nonlocal elasticity, the stress at reference point, x, in an elastic body not only depends on the strains at x, but also on the strains at all other points of the body. The constitutive equations, based on Eringen's nonlocal elasticity, are expressed as [26,27]:

$$\begin{Bmatrix} \sigma_{xx} \\ \sigma_{\theta\theta} \\ \sigma_{x\theta} \\ \sigma_{\theta z} \\ \sigma_{xz} \end{Bmatrix} - (e_0 a)^2 \nabla^2 \begin{Bmatrix} \sigma_{xx} \\ \sigma_{\theta\theta} \\ \sigma_{x\theta} \\ \sigma_{\theta z} \\ \sigma_{xz} \end{Bmatrix} = \begin{bmatrix} \frac{E}{1-v^2} & \frac{vE}{1-v^2} & 0 & 0 & 0 \\ \frac{vE}{1-v^2} & \frac{E}{1-v^2} & 0 & 0 & 0 \\ 0 & 0 & G & 0 & 0 \\ 0 & 0 & 0 & G & 0 \\ 0 & 0 & 0 & 0 & G \end{bmatrix} \begin{Bmatrix} \varepsilon_{xx} \\ \varepsilon_{\theta\theta} \\ \gamma_{x\theta} \\ \gamma_{\theta z} \\ \gamma_{xz} \end{Bmatrix}, \quad (1)$$

where E, G and v are Young's modulus, shear modulus and Poisson's ratio, respectively, and $e_0 a$ denotes the nonlocal parameter, which leads to consider the small scale effect. Let u_x, u_y and u_z be the three-dimensional displacement components in the x, θ and z directions,

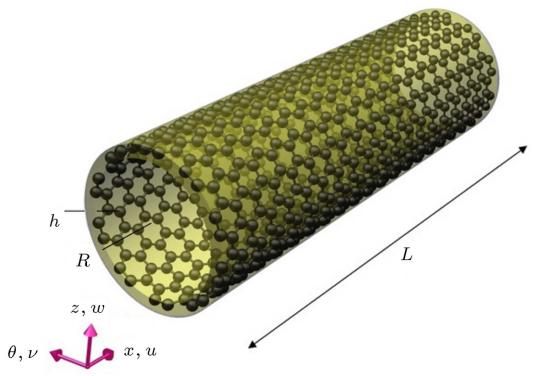

Figure 1. Schematic of a single-walled BNNT treated as an elastic cylindrical shell.

respectively. They can be defined as:

$$u_x(x,\theta,z,t) = u(x,\theta,t) + z\psi_x(x,\theta,t), \quad (2a)$$

$$u_y(x,\theta,z,t) = v(x,\theta,t) + z\psi_\theta(x,\theta,t), \quad (2b)$$

$$u_z(x,\theta,z,t) = w(x,\theta,z,t), \quad (2c)$$

where u, v and w are the reference surface displacements and ψ_x and ψ_θ are the rotations of transverse normal about the x-axis and y-axis, respectively. The mid-surface strains and curvature changes are given by:

$$\varepsilon_{xx} = \frac{\partial u}{\partial x}, \qquad \varepsilon_{\theta\theta} = \frac{1}{R}\frac{\partial v}{\partial \theta} + \frac{w}{R},$$

$$\gamma_{x\theta} = \frac{\partial v}{\partial x} + \frac{1}{R}\frac{\partial u}{\partial \theta}, \qquad \gamma_{xz} = \frac{\partial w}{\partial x} + \psi_x,$$

$$\gamma_{\theta z} = \frac{1}{R}\frac{\partial w}{\partial \theta} - \frac{v}{R} + \psi_\theta, \quad (3a)$$

$$k_x = \frac{\partial \psi_x}{\partial x}, \qquad k_\theta = \frac{1}{R}\frac{\partial \psi_\theta}{\partial \theta}, \qquad k_{x\theta} = \frac{\partial \psi_\theta}{\partial x} + \frac{1}{R}\frac{\partial \psi_x}{\partial \theta}. \quad (3b)$$

Using Eqs. (1) to (3), the stress and moment resultants can be given as follows:

$$N_{xx} = \int_{-h/2}^{h/2} \sigma_{xx} dz, \qquad \text{i.e.,}$$

$$N_{xx} - (e_0 a)^2 \nabla^2 N_{xx} = \frac{Eh}{1-v^2}\frac{\partial u}{\partial x} + \frac{vEh}{1-v^2}\left(\frac{1}{R}\frac{\partial v}{\partial \theta} + \frac{w}{R}\right), \quad (4a)$$

$$N_{\theta\theta} = \int_{-h/2}^{h/2} \sigma_{\theta\theta} dz, \qquad \text{i.e.}$$

$$N_{\theta\theta} - (e_0 a)^2 \nabla^2 N_{\theta\theta} = \frac{vEh}{1-v^2}\frac{\partial u}{\partial x} + \frac{Eh}{1-v^2}\left(\frac{1}{R}\frac{\partial v}{\partial \theta} + \frac{w}{R}\right), \quad (4b)$$

$$N_{x\theta} = \int_{-h/2}^{h/2} \sigma_{x\theta} dz, \qquad \text{i.e.,}$$

$$N_{x\theta} - (e_0 a)^2 \nabla^2 N_{x\theta} = Gh\left(\frac{\partial v}{\partial x} + \frac{1}{R}\frac{\partial u}{\partial \theta}\right), \quad (4c)$$

$$M_{xx} = \int_{-h/2}^{h/2} z\sigma_{xx} dz, \qquad \text{i.e.,}$$

$$M_{xx} - (e_0 a)^2 \nabla^2 M_{xx} = D\left(\frac{\partial \psi_x}{\partial x} + \frac{v}{R}\frac{\partial \psi_\theta}{\partial \theta}\right), \quad (4d)$$

$$M_{\theta\theta} = \int_{-h/2}^{h/2} z\sigma_{\theta\theta}dz, \qquad \text{i.e.,}$$

$$M_{\theta\theta} - (e_0a)^2\nabla^2 M_{\theta\theta} = D\left(\frac{1}{R}\frac{\partial\psi_\theta}{\partial\theta} + \upsilon\frac{\partial\psi_x}{\partial x}\right), \quad (4e)$$

$$M_{x\theta} = \int_{-h/2}^{h/2} z\sigma_{x\theta}dz, \qquad \text{i.e.,}$$

$$M_{x\theta} - (e_0a)^2\nabla^2 M_{x\theta} = \frac{1}{2}D(1-\upsilon)\left(\frac{\partial\psi_\theta}{\partial x} + \frac{1}{R}\frac{\partial\psi_x}{\partial\theta}\right), \quad (4f)$$

$$Q_{xx} = \int_{-h/2}^{h/2} \sigma_{xz}dz, \qquad \text{i.e.,}$$

$$Q_{xx} - (e_0a)^2\nabla^2 Q_{xx} = Gh\left(\frac{\partial w}{\partial x} + \psi_x\right), \quad (4g)$$

$$Q_{\theta\theta} = \int_{-h/2}^{h/2} \sigma_{\theta z}dz, \qquad \text{i.e.,}$$

$$Q_{\theta\theta} - (e_0a)^2\nabla^2 Q_{\theta\theta} = Gh\left(\frac{1}{R}\frac{\partial w}{\partial\theta} - \frac{v}{R} + \psi_\theta\right), \quad (4h)$$

where D is the bending rigidity. The governing equations for cylindrical shells, in terms of force and moment resultants, based on the Donnell theory, are given by [38]:

$$\frac{\partial N_{xx}}{\partial x} + \frac{1}{R}\frac{\partial N_{x\theta}}{\partial\theta} = 0, \quad (5a)$$

$$\frac{\partial N_{x\theta}}{\partial x} + \frac{1}{R}\frac{\partial N_{\theta\theta}}{\partial\theta} + \frac{Q_{\theta\theta}}{R} = 0, \quad (5b)$$

$$\frac{\partial Q_{xx}}{\partial x} + \frac{1}{R}\frac{\partial Q_{\theta\theta}}{\partial\theta} - \frac{N_{\theta\theta}}{R} - P\frac{\partial^2 w}{\partial x^2} = 0, \quad (5c)$$

$$\frac{\partial M_{xx}}{\partial x} + \frac{1}{R}\frac{\partial M_{x\theta}}{\partial\theta} - Q_{xx} = 0, \quad (5d)$$

$$\frac{\partial M_{x\theta}}{\partial x} + \frac{1}{R}\frac{\partial M_{\theta\theta}}{\partial\theta} - Q_{\theta\theta} = 0, \quad (5e)$$

where P represents the applied axial load. Eqs. (5) are multiplied by $(1-(e_0a)^2\nabla^2)$. The left hand side of the resulting equations can be derived by Eqs. (4) and the right hand side can be written easily. Thus, the field equations can be expressed as:

$$\frac{Eh}{1-\upsilon^2}u_{,xx} - \frac{1}{2}\left(\frac{1}{R}\right)^2\frac{Eh}{2(1+\upsilon)}u_{,\theta\theta} + \frac{1}{R}\left(\frac{\upsilon Eh}{1-\upsilon^2} + \frac{1}{2}\frac{Eh}{2(1+\upsilon)}\right)v_{,x\theta} + \frac{1}{R}\frac{\upsilon Eh}{1-\upsilon^2}w_{,x} = 0, \quad (6a)$$

$$\frac{1}{R}\left(\frac{\upsilon Eh}{1-\upsilon^2} + \frac{1}{2}\frac{Eh}{2(1+\upsilon)}\right)u_{,x\theta} + \frac{1}{2}\frac{Eh}{2(1+\upsilon)}v_{,xx} - \left(\frac{1}{R}\right)^2\frac{Eh}{1-\upsilon^2}v_{,\theta\theta} - \frac{Gh}{R^2}v - \left(\frac{1}{R}\right)^2\left(\frac{Eh}{1-\upsilon^2} + Gh\right)w_{,\theta} + \frac{Gh}{R}\psi_\theta = 0, \quad (6b)$$

$$-\frac{1}{R}\frac{\upsilon Eh}{1-\upsilon^2}u_{,x} + \left(\frac{1}{R}\right)^2\left(\frac{Eh}{1-\upsilon^2} + Gh\right)v_{,\theta} + Ghw_{,xx} - \left(\frac{1}{R}\right)^2 Ghw_{,\theta\theta} - \left(\frac{1}{R}\right)^2\frac{Eh}{1-\upsilon^2}w + Gh\psi_{x,x} + \frac{Gh}{R}\psi_{\theta,\theta} = P\left[w_{,xx} - (e_0a)^2\left(w_{,xxxx} + \frac{1}{R^2}w_{,xx\theta\theta}\right)\right], \quad (6c)$$

$$-Ghw_{,x} + D\psi_{x,xx} + \frac{1}{2}\left(\frac{1}{R}\right)^2\frac{(1-\upsilon)D}{2}\psi_{x,\theta\theta} - Gh\psi_x + \frac{1}{R}\left(\upsilon D + \frac{1}{2}\frac{(1-\upsilon)D}{2}\right)\psi_{\theta,x\theta} = 0, \quad (6d)$$

$$\frac{Gh}{R}v + \frac{Gh}{R}w_{,\theta} + \frac{1}{R}\left(\upsilon D + \frac{1}{2}\frac{(1-\upsilon)D}{2}\right)\psi_{x,x\theta} + \frac{1}{2}\frac{(1-\upsilon)D}{2}\psi_{\theta,xx} + \left(\frac{1}{R}\right)^2 D\psi_{\theta,\theta\theta} - Gh\psi_\theta = 0. \quad (6e)$$

Here, the Rayleigh-Ritz method is used to obtain the critical axial buckling load of BNNTs. In order to apply the Rayleigh-Rayleigh-Ritz method, it is first necessary to obtain the variational statement equivalent to the partial differential equations that are governed by the buckling of BNNTs (Eqs. (6)). The variational form equivalent to Donnell-type buckling equations is constructed as follows:

$$\Pi(u,v,w,\psi_x,\psi_\theta) = \frac{1}{2}\int_0^T\int_\Omega\left(\left[\frac{Eh}{1-\upsilon^2}u_{,x} + \frac{1}{R}\frac{\upsilon Eh}{1-\upsilon^2}(v_{,\theta}+w)\right]u_{,x} + \left[\frac{\upsilon Eh}{1-\upsilon^2}u_{,x} + \frac{1}{R}\frac{Eh}{1-\upsilon^2}(v_{,\theta}+w)\right]\frac{1}{R}(v_{,\theta}+w)\right.$$

$$+\frac{Eh}{2(1+\upsilon)}\left(\frac{u_{,\theta}}{R}+v_{,x}\right)+D\left(\psi_{x_{,x}}+\frac{\upsilon}{R}\psi_{\theta_{,\theta}}\right)\psi_{x_{,x}}$$

$$+\frac{D}{R}\left(\upsilon\psi_{x_{,x}}+\frac{1}{R}\psi_{\theta_{,\theta}}\right)\psi_{\theta_{,\theta}}$$

$$+\frac{(1-\upsilon)D}{2}\left(\frac{\psi_{x_{,\theta}}}{R}+\psi_{\theta_{,x}}\right)^2+\frac{Eh}{2(1+\upsilon)}(w_{,x}+\psi_x)^2$$

$$+\frac{Eh}{2(1+\upsilon)}\left(-\frac{v}{R}+\frac{w_{,\theta}}{R}+\psi_\theta\right)^2\Bigg)d\Omega dt$$

$$+\frac{1}{2}\int_0^T\int_\Omega P\Bigg((w_{,x})^2$$

$$-(e_0a)^2\left[\left(w_{,xx}+\frac{1}{R^2}w_{,\theta\theta}\right)w_{,xx}\right]\Bigg)d\Omega dt. \tag{7}$$

In order to approximate the buckling mode shapes corresponding to various end conditions, one can assume the functions of the polynomial series as:

$$u(x,\theta)=U(x)\sin(n\theta), \tag{8a}$$

$$v(x,\theta)=V(x)\cos(n\theta), \tag{8b}$$

$$w(x,\theta)=W(x)\sin(n\theta), \tag{8c}$$

$$\psi_x(x,\theta)=\Psi_x(x)\sin(n\theta), \tag{8d}$$

$$\psi_\theta(x,\theta)=\Psi_\theta(x)\cos(n\theta), \tag{8e}$$

where:

$$U(x)=\left(\sum_{e=1}^{M}A_ex^{e-1}\right)(x)^{n_u^0}(L-x)^{n_u^L}=\sum_{e=1}^{M}A_eU_e, \tag{9a}$$

$$V(x)=\left(\sum_{e=1}^{M}B_ex^{e-1}\right)(x)^{n_v^0}(L-x)^{n_v^L}=\sum_{e=1}^{M}B_eV_e, \tag{9b}$$

$$W(x)=\left(\sum_{e=1}^{M}C_ex^{e-1}\right)(x)^{n_w^0}(L-x)^{n_w^L}=\sum_{e=1}^{M}C_eW_e, \tag{9c}$$

$$\Psi_x(x)=\left(\sum_{e=1}^{M}D_ex^{e-1}\right)(x)^{n_{\psi x}^0}(L-x)^{n_{\psi x}^L}$$

$$=\sum_{e=1}^{M}D_e\Psi_{x_e}, \tag{9d}$$

Table 1. Values of n_u, n_v, n_w, n_{ψ_x} and n_{ψ_θ} for different boundary conditions.

Boundary conditions	n_u	n_v	n_w	n_{ψ_x}	n_{ψ_θ}
Simply supported end	0	1	1	0	1
Clamped end	1	1	2	1	1
Free end	0	0	0	0	0

$$\Psi_\theta(x)=\left(\sum_{e=1}^{M}E_ex^{e-1}\right)(x)^{n_{\psi\theta}^0}(L-x)^{n_{\psi\theta}^L}$$

$$=\sum_{e=1}^{M}E_e\Psi_{\theta_e}, \tag{9e}$$

in which M is the number of terms of the polynomial series. The values of n_u, n_v, n_w, n_{ψ_x} and n_{ψ_x} are given in Table 1, corresponding to different boundary conditions. The superscripts of the powers, i.e. 0 and L, correspond to the boundary conditions of the nanotube at $x=0$ and $x=L$, respectively, and $A_e^{(i)}$, $B_e^{(i)}$, $C_e^{(i)}$, $D_e^{(i)}$ and $E_e^{(i)}$ are the generalized amplitudes. Substituting Eqs. (8) into Eq. (7), and then using the Rayleigh-Ritz technique, one can have:

$$\frac{\partial\Pi}{\partial A_e}=\frac{\partial\Pi}{\partial B_e}=\frac{\partial\Pi}{\partial C_e}=\frac{\partial\Pi}{\partial D_e}=\frac{\partial\Pi}{\partial E_e}=0. \tag{10}$$

Eq. (10) leads to an eigenvalue problem with the critical buckling load of BNNTs as the eigenvalue parameter.

3. Mechanical properties of BNNTs

3.1. Molecular mechanics modeling

In the context of molecular mechanics theory, by the use of Hooke's law to characterize the interactions between bound atoms in a single-walled BNNT, the general expression of total potential energy, V_t, can be given as the sum of several individual energy terms:

$$V_t=\sum\frac{1}{2}K_\rho(dr)^2+\sum\frac{1}{2}C_\theta(d\theta)^2, \tag{11}$$

where dr and $d\theta$ are the bond elongation and bond angle variance, respectively. The force constants, K_ρ and C_θ, are corresponding to the energies of bond stretching and bond angle variation, respectively. To obtain the equilibrium equations using molecular mechanics theory, the structure of the system can be modeled as an effective "stick-spiral" system. In this system, one can use an elastic stick with an axial stiffness of K_ρ to model the force-stretch relationship of the B-N bond, and a spiral spring with a stiffness of C_θ to model the twisting moment resulting from an angular distortion of the bond angle. It should be remarked that the bending rigidity of the stick is assumed to be infinite, since the

chemical bond always remains straight, regardless of the applied load.

Following the treatment in [25] and making use of the molecular mechanics conceptions by manipulating the resulting relations, the following analytical expressions for effective in-plane stiffness and Poisson's ratio of an (n, m) nanotube can be obtained:

$$(Eh)_{\text{eff}} = \frac{1}{2\pi R} \left(\frac{(n+m)K_\rho r_1}{\sin\left(\frac{\pi}{3}+\Theta\right)\sin\left(\frac{\theta_3}{2}\right)\left(\frac{\lambda_A K_\rho r_1^2}{C_\theta \tan\left(\frac{\theta_3}{2}\right)^2+1}\right)} \right), \quad (12)$$

$$\upsilon = -\frac{\cos\left(\frac{\theta_3}{2}\right)\left(1-\frac{\lambda_A K_\rho r_1^2}{C_\theta}\right)}{\left(1+\cos\left(\frac{\theta_3}{2}\right)\right)\left(\frac{\lambda_A K_\rho r_1^2}{C_\theta \tan\left(\frac{\theta_3}{2}\right)^2}+1\right)}, \quad (13)$$

where:

$$\lambda_A = \frac{\sin(\theta_2)\cot\left(\frac{\theta_3}{2}\right)}{4\sin(\theta_2)\cot\left(\frac{\theta_3}{2}\right) - 2\sin\left(\frac{\theta_3}{2}\right)\cot(\theta_2)\cos\left(\frac{\pi}{n+m}\right)}.$$

Here, Θ is the chiral angle, and r_1 and θ_2 are θ_3 bond length and bond angles (see Figure 2). It should be noted that the foregoing formulas reduce to those obtained in [22] for armchair and zigzag nanotubes by setting $n = m$ and $m = 0$, respectively.

3.2. DFT calculations

To determine the mechanical properties of BNNTs via Eqs. (12) and (13) in an accurate way, it is necessary to apply the proper force constants (K_ρ and C_θ), whose values can be quantified by establishing a link between the several individual energy terms from molecular mechanics modeling, as illustrated in Figure 3, and the strain energy of a nanotube calculated, based on the density functional theory. The reader is referred to [25] regarding the basic equations of the density functional theory and further details on this approach.

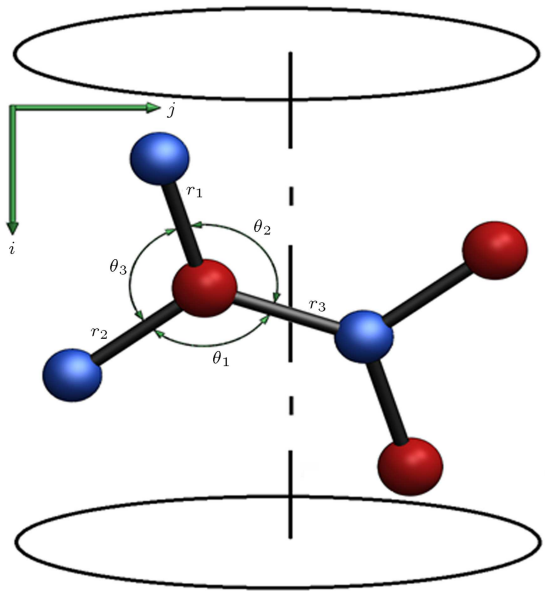

Figure 2. Three bond lengths and three bond angles in a boron nitride nanotube.

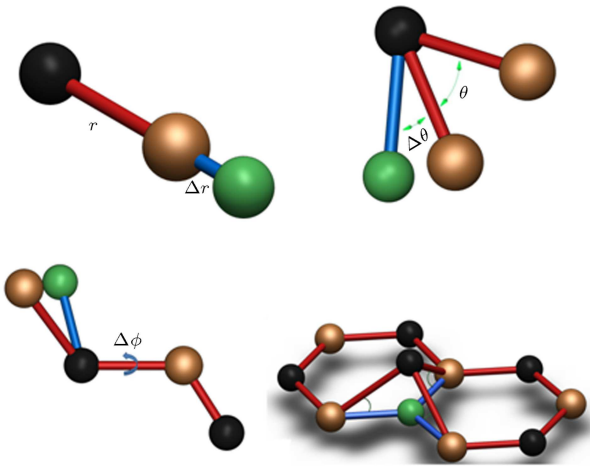

Figure 3. Different bond structures of an h-BN cell corresponding to each energy term.

Within the framework of the generalized gradient approximation (GGA), the exchange correlation of Perdew-Burke-Ernzerhof (PBE) [39,40] is adopted to perform the DFT calculations in this work. The Quantum-Espresso code [41] is applied to perform simulations of the analysis. The previous first principle study demonstrated that the results are insensitive to the increasing of the unit cell dimension [42]. Therefore, for convenience, the unit cell used in the calculations performed herein is assumed to be the smallest hexagonal one. Brillouin zone integration is implemented with a Monkhorst-Pack [43] k-point mesh of $20 \times 20 \times 1$, and the cut-off energy for plane wave expansion is selected to be 80 Ry.

From the present DFT calculations, the force constants, K_ρ and C_θ, are evaluated to be 620.47 nN/nm and 1.05 nN nm, respectively. Also, the value of the effective bending stiffness, D, of BNNT, obtained from the DFT calculations, is 0.64 eV.

4. Numerical results and discussion

Table 2 provides a comparison between the calculated in-plane stiffness in this study with those reported in previous work by different methods. It is observed that the prediction of the present approach is in good agreement with other studies. Furthermore, Table 3 shows the elastic properties of achiral (armchair and zigzag) BNNTs obtained by the present study and Hernandez et al. [11]. The agreement between the

Table 2. Comparison of the average calculated in-plane stiffness of BNNTs by the present work and previous studies.

Reference	Method	$(Eh)_{\text{eff}}$ (TPa nm)
Present study	Molecular mechanics	0.280
Griebel et al. [10]	Molecular dynamics	0.248-0.292
Hernandez et al. [11]	Tight-binding	0.3
Kudin et al. [13]	Ab initio	0.271
Baumeier et al. [16]	Ab initio	0.279
Oh [17]	Continuum lattice approach	0.322
Jiang and Guo [18]	Molecular mechanics	0.26-0.269

Table 3. In-plane stiffness and Poisson's ratio of achiral BNNTs obtained from the present work and those of [11].

(n,m)	$(Eh)_{\text{eff}}$ (TPa nm)	Difference percentage	υ	Difference percentage
(10,0)	0.284[a] 0.27761[b]	2.25%	0.232[a] 0.22503[b]	3.00%
(6,6)	0.296[a] 0.27917[b]	5.92%	0.268[a] 0.22070[b]	22.83%
(15,0)	0.298[a] 0.28032[b]	5.93%	0.246[a] 0.21749[b]	11.58%
(10,10)	0.306[a] 0.28133[b]	8.06%	0.263[a] 0.21465[b]	18.38%
(20,0)	0.301[a] 0.28130[b]	6.54%	0.254[a] 0.21475[b]	15.45%
(15,15)	0.310[a] 0.28202[b]	9.02%	0.263[a] 0.21272[b]	19.11%

[a]: [11]; [b]: Present.

Table 4. In-plane stiffness and Poisson's ratio of chiral BNNTs.

(n,m)	$(Eh)_{\text{eff}}$ (TPa nm)	υ
(15,3)	0.28071	0.21617
(18,3)	0.28122	0.21482
(19,2)	0.28127	0.21472
(14,11)	0.28174	0.21350
(14,7)	0.28126	0.21475
(20,10)	0.28193	0.21293
(30,15)	0.28229	0.21194
(19,17)	0.28219	0.21226
(19,18)	0.28221	0.21219

two sets of results appears to be sufficient to qualify the present analytical formulae as precise and powerful tools for obtaining the elastic properties of BNNTs. The results of chiral BNNTs are also presented in Table 4.

Using the present combined model, the critical buckling loads for armchair, zigzag and chiral single-walled BNNTs subject to clamped boundary conditions are tabulated in Table 5. The results in this table show that by increasing tube diameter, the critical buckling load tends to be increased.

Table 5. Critical buckling load of clamped single-walled BNNTs with different chiralities ($L/D = 10$ and $e_0 a = 1$ nm).

Armchair		Zigzag		Chiral	
(7,7)	12.7687	(10,0)	7.5652	(7,4)	6.8605
(10,10)	29.6669	(15,0)	22.0720	(15,3)	28.7507
(12,12)	34.5031	(20,0)	33.4503	(13,9)	32.2935
(15,15)	40.8159	(25,0)	39.7077	(18,3)	33.0034
(20,20)	49.0149	(30,0)	44.9560	(19,2)	33.5515
(25,25)	54.8772	(35,0)	49.2975	(18,4)	33.8522
(30,30)	59.1286	(40,0)	52.8689	(14,11)	35.6997

Figure 4 illustrates the variations of the critical buckling load versus various aspect ratios of a (18,9) single-walled BNNT ($(Eh)_{\text{eff}} = 0.28178$ TPa nm, $\upsilon = 0.21334$) under different boundary conditions. As expected, end conditions will have an important effect on the critical buckling load. It can be seen in the figure that two different types of buckling are distinguishable.

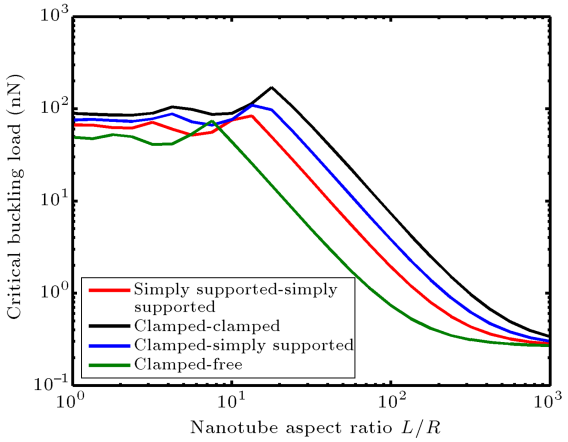

Figure 4. Variation of critical buckling load of a (18,9) single-walled BNNT with aspect ratio for different boundary conditions.

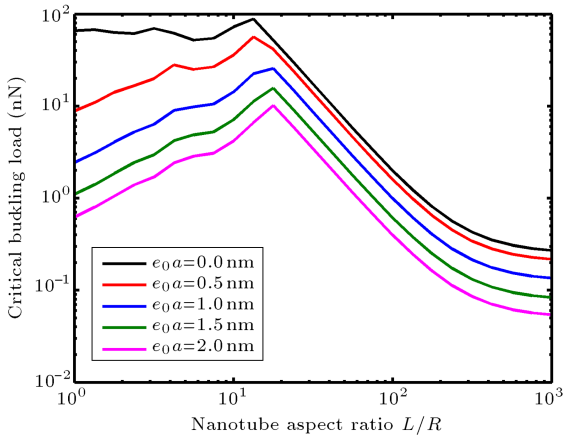

Figure 5. Variation of critical buckling load of a (25,0) single-walled BNNT with aspect ratio for different nonlocal parameters.

The L/R ratios smaller than, approximately, 13.3, 17.8, 17.9 and 7.5, for simply supported-simply supported, clamped-clamped, clamped-simply supported and clamped-free end conditions, respectively, correspond to the shell-like buckling, while for greater values above L/R ratios, column-like buckling takes place. It should be noted that, unlike column-like buckling, the effect of aspect ratio on the case of shell-like buckling is almost negligible.

In Figure 5, the critical buckling loads for a (25,0) single-walled BNNT with simply supported ends ($(Eh)_{\text{eff}} = 0.28176$ TPa nm, $\upsilon = 0.21347$), corresponding to various nonlocal parameters ranging from $e_0a = 0$ (corresponding to the classical/ local continuum model) to $e_0a = 2$ nm, are shown with respect to different aspect ratios. From this figure, one can deduce that for short length BNNTs, for which shell-like buckling is dominant, the small length scale has a profound effect on the critical buckling loads, particularly for higher values of nonlocal parameter.

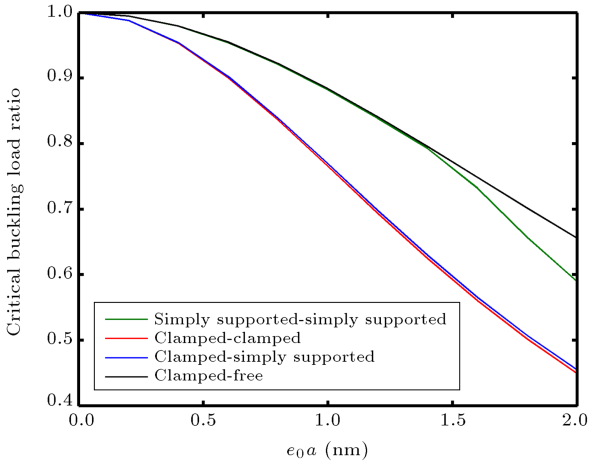

Figure 6. Critical buckling load ratio for a (80,80) single-walled BNNT with different boundary conditions ($L/R = 10$).

As the aspect ratio increases, the effect of small length scale diminishes.

To further investigate small scale and boundary condition effects, Figuer 6 shows the ratio of nonlocal critical buckling load to the local one, versus the nonlocal parameter for a (80,80) single-walled BNNT ($(Eh)_{\text{eff}} = 0.28257$ TPa nm, $\upsilon = 0.21121$) subject to different boundary conditions. As can be observed from this figure, the effect of small length scale on the critical buckling load depends on the magnitude of the nonlocal parameter, as well as the type of boundary condition selected. One can find that the effect of boundary conditions is more pronounced for higher values of the nonlocal parameter. Moreover, by increasing the nonlocal parameter, the critical buckling load obtained from the nonlocal shell model will have a lower value compared to that from the local one. It is further observed that the nonlocal influence is more prominent for stiffer boundary conditions.

5. Concluding remarks

The axial buckling of single-walled BNNTs subject to different boundary conditions was studied in this work. A hybrid continuum-atomistic model was developed to obtain the critical axial buckling loads of chiral BNNTs. Based on nonlocal elasticity, nonlocal shell theory was employed to derive the governing equations. Within the framework of calculus of variation, the Rayleigh-Ritz approach with polynomial series was applied to the variational form of governing equations. The molecular mechanics theory was used in conjunction with the density functional theory to obtain the exact values of effective in-plane and bending stiffnesses and Poisson's ratio of single-walled BNNTs. Good agreement, observed in a comparison between the present results for the mechanical properties of BNNTs and

those from existing data from the literature, confirm the validity of the present solution method. With respect to the numerical results, the significance of the small size effects on critical buckling load was shown to be dependent on the geometric sizes and boundary conditions of BNNTs.

References

1. Ciofani, G., Raffaa, V., Menciassi, A. and Cuschieri, A. "Boron nitride nanotubes: An innovative tool for nanomedicine", *Nano Today*, **4**, pp. 8-10 (2009).
2. Rubio, A., Corkill, J.L. and Cohen, M.L. "Theory of graphitic boron nitride nanotubes", *Phys. Rev. B*, **49**, pp. 5081-5084 (1994).
3. Blase, X., Rubio, A., Louie, S.G. and Cohen, M.L. "Stability and band gap constancy of boron nitride nanotubes", *Europhys. Lett.*, **28**, pp. 335-340 (1994).
4. Chopra, N.G., Luyken, R.J., Cherrey, K., Crespi, V.H., Cohen, M.L., Louie, S.G. and Zettl, A. "Boron nitride nanotubes", *Science*, **269**, pp. 966-967 (1995).
5. Kim, P., Shi, L., Majumdar, A. and McEuen, P.L. "Thermal transport measurements of individual multiwalled nanotubes", *Phys. Rev. Lett.*, **87**, p. 2155021 (2001).
6. Zhang, Z.H., Guo, W.L. and Dai, Y.T. "Stability and electronic properties of small boron nitride nanotubes", *J. Appl. Phys.*, **105**, p. 084312 (2009).
7. Zhang, Z.H. and Guo, W.L. "Tunable ferromagnetic spin ordering in boron nitride nanotubes with topological fluorine adsorption", *J. Am. Chem. Soc.*, **131**, pp. 6874-6879 (2009).
8. Sai, N. and Mele, E.J. "Microscopic theory for nanotube piezoelectricity", *Phys. Rev. B*, **68**, p. 241405 (2003).
9. Chen, Y., Zou, J., Campbell, S.J. and Caer, G.L. "Boron nitride nanotubes: Pronounced resistance to oxidation", *Appl. Phys. Lett.*, **84**, pp. 2430-2432 (2004).
10. Griebel, M., Hamaekers, J. and Heber, F. "A molecular dynamics study on the impact of defects and functionalization on the Young modulus of boron-nitride nanotubes", *Comput. Mater. Sci.*, **45**, pp. 1097-1103 (2009).
11. Hernandez, E., Goze, C., Bernier, P. and Rubio, A. "Elastic properties of C and BxCyNz composite nanotubes", *Phys. Rev. Lett.*, **80**, pp. 4502-4505 (1998).
12. Vaccarini, L., Goze, C., Henrard, L., Hernandez, E., Bernier, P. and Rubio, A. "Mechanical and electronic properties of carbon and boron-nitride nanotubes", *Carbon*, **38**, pp. 1681-1690 (2000).
13. Kudin, K.N., Scuseria, G.E. and Yakobson, B.I. "C2F, BN, and C nanoshell elasticity from ab initio computations", *Phys. Rev. B*, **64**, pp. 235406-235416 (2001).
14. Akdim, B., Pachter, R., Duan, X.F. and Adams, W.W. "Comparative theoretical study of single-wall carbon and boron-nitride nanotubes", *Phys. Rev. B*, **67**, p. 245404 (2003).
15. Gou, G.Y., Pan, B.C. and Shi, L. "Theoretical study of size-dependent properties of BN nanotubes with intrinsic defects", *Phys. Rev. B*, **76**, p. 155414 (2007).
16. Baumeier, B., Kruger, P. and Pollmann, J. "Structural, elastic, and electronic properties of SiC, BN, and BeO nanotubes", *Phys. Rev. B*, **76**, p. 085407 (2007).
17. Oh, E.S. "Elastic properties of boron-nitride nanotubes through the continuum lattice approach", *Mater. Lett.*, **64**, pp. 859-862 (2010).
18. Jiang, L. and Guo, W. "A molecular mechanics study on size-dependent elastic properties of single-walled boron nitride nanotubes", *J. Mech. Phys. Solids*, **59**, pp. 1204-1213 (2011).
19. Chopra, N.G. and Zettl, A. "Measurement of the elastic modulus of a multi-wall boron nitride nanotube", *Solid State Commun.*, **105**, pp. 297-300 (1998).
20. Xiang, H.J., Yang, J., Hou, J.G. and Zhu, Q. "First-principles study of small-radius single-walled BN nanotubes", *Phys. Rev. B*, **68**, p. 035427 (2003).
21. Golberg, D., Bando, Y., Huang, Y., Terao, T., Mitome, M., Tang, C. and Zhi, C. "Boron nitride nanotubes and nanosheets", *ACS Nano*, **4**, pp. 2979-2993 (2010).
22. Chang, T. and Gao, H. "Size-dependent elastic properties of a single-walled carbon nanotube via a molecular mechanics model", *J. Mech. Phys. Solids*, **51**, pp. 1059-1074 (2003).
23. Shen, L. and Li, J. "Transversely isotropic elastic properties of single-walled carbon nanotubes", *Phys. Rev. B*, **69**, p. 045414 (2004).
24. Natsuki, T., Tantrakarn, K. and Endo, M. "Prediction of elastic properties for single-walled carbon nanotubes", *Carbon*, **42**, pp. 39-45 (2004).
25. Mirnezhad, M., Ansari, R. and Rouhi, H. "Effects of hydrogen adsorption on mechanical properties of chiral single-walled zinc oxide nanotubes", *J. Appl. Phys.*, **111**, p. 014308 (2012).
26. Eringen, A.C. "On differential quations of nonlocal elasticity and solutions of screw dislocation and surface waves", *J. Appl. Phys.*, **54**, pp. 4703-4710 (1983).
27. Eringen, A.C., *Nonlocal Continuum Field Theories*, Springer, New York (2002).
28. Peddieson, J., Buchanan, G.R. and McNitt, R.P. "Application of nonlocal continuum models to nanotechnology", *Int. J. Eng. Sci.*, **41**, pp. 305-312 (2003).
29. Sudak, L.J. "Column buckling of multiwalled carbon nanotubes using nonlocal continuum mechanics", *J. Appl. Phys.*, **94**, pp. 7281-7287 (2003).
30. Wang, C.M., Zhang, Y.Y., Ramesh, S.S. and Kitipornchai, S. "Buckling analysis of micro- and nanorods/tubes based on nonlocal Timoshenko beam theory", *J. Phys. D: Appl. Phys.*, **39**, pp. 3904-3909 (2006).

31. Li, R. and Kardomateas, G.A. "Thermal buckling of multi-walled carbon nanotubes by nonlocal elasticity", *ASME J. Appl. Mech.*, **74**, pp. 399-405 (2007).

32. Challamel, N. and Wang, C.M. "The small length scale effect for a non-Local cantilever beam: a paradox solved", *Nanotechnology*, **19**, p. 345703 (2008).

33. Wang, L. "Vibration and instability analysis of tubular nano- and micro-beams conveying fluid using nonlocal elastic theory", *Physica E*, **41**, pp. 1835-1840 (2009).

34. Roque, C.M.C., Ferreira, A.J.M. and Reddy, J.N. "Analysis of Timoshenko nanobeams with a nonlocal formulation and meshless method", *Int. J. Eng. Sci.*, **49**, pp. 976-984 (2011).

35. Narendar, S., Roy Mahapatra, D. and Gopalakrishnan, S. "Prediction of nonlocal scaling parameter for armchair and zigzag single-walled carbon nanotubes based on molecular structural mechanics, nonlocal elasticity and wave propagation", *Int. J. Eng. Sci.*, **49**, pp. 509-522 (2011).

36. Ansari, R., Gholami, R. and Sahmani, S. "On the dynamic stability of embedded single-walled carbon nanotubes including thermal environment effects", *Scientia Iranica*, **19**, pp. 919-925 (2012).

37. Ansari, R. and Rouhi, H. "Analytical treatment of the free vibration of single-walled carbon nanotubes based on the nonlocal flugge shell theory", *ASME J. Eng. Mater. Technol.*, **134**, p. 011008 (2012).

38. Donnell, L.H., *Beam, Plates and Shells*, McGraw-Hill, New York (1976).

39. Perdew, J.P., Burke, K. and Ernzerhof, M. "Generalized gradient approximation made simple", *Phys. Rev. Lett.*, **77**, pp. 3865-3868 (1996).

40. Perdew, J.P., Burke, K. and Wang, Y. "Generalized gradient approximation for the exchange-correlation hole of a many-electron system", *Phys. Rev. B*, **54**, pp. 16533-16539 (1996).

41. Baroni, S., Corso, D.A., Gironcoli, S., Giannozzi, P., Cavazzoni, C., Ballabio, G., Scandolo, S., Chiarotti, G., Focher, P., Pasquarello, A., Laasonen, K., Trave, A., Car, R., Marzari, N. and Kokalj, A., http://www.pwscf.org/.

42. Topsakal, M., Cahangirov, S. and Ciraci, S. "The response of mechanical and electronic properties of graphane to the elastic strain", *Appl. Phys. Lett.*, **96**, p. 091912 (2010).

43. Monkhorst, H.J. and Pack, J.D. "Special points for brillouin-zone integrations", *Phys. Rev. B*, **13**, pp. 5188-5192 (1976).

Biographies

Reza Ansari received his PhD degree, in 2008, from the University of Guilan, Iran, where he is currently Faculty member in the Department of Mechanical Engineering. He was also a visiting fellow at Wollongong University, Australia, from 2006-2007. He has authored numerous refereed journal papers and book chapters. His research interests include computational nano- and micro-mechanics, advanced numerical techniques, nonlinear analyses and prediction of the mechanical behavior of smart composite/FGM shell-type structures.

Hessam Rouhi received his BS and MS degrees in Mechanical Engineering, in 2008 and 2011, respectively, from the University of Guilan, Iran, where he is currently a PhD student in Mechanical Engineering. His research interests include: computational nanomechanics and the mechanical behavior of structures, including buckling and vibration.

Mahdi Mirnezhad received his BS degree in Mechanical Engineering from Ferdowsi University of Mashhad, Iran, in 2008, and his MS degree from the University of Guilan, Iran, in 2011. His research interests include quantum mechanics, molecular mechanics and mechanical properties of nanostructures.